Organic linker defines the excited-state decay of photocatalytic MIL-125(Ti)-type materials

Garcia Santaclara, J; Nasalevich, M; Castellanos Ortega, S; Evers, WH; Spoor, FCM; Siebbeles, LDA; Kapteijn, F; Grozema, FC; Houtepen, AJ; Gascon, J

DOI
10.1002/cssc.201501353

Publication date
2016

Document Version
Final published version

Published in
ChemSusChem (online)

ChemPubSoc Europe

DOI: 10.1002/cssc.201501353

CHEMSUSCHEM Full Papers

Organic Linker Defines the Excited-State Decay of Photocatalytic MIL-125(Ti)-Type Materials

Jara G. Santaclara[+],[a] Maxim A. Nasalevich[+],[a] Sonia Castellanos,[a] Wiel H. Evers,[b, c] Frank C. M. Spoor,[b] Kamila Rock,[d] Laurens D. A. Siebbeles,[b] Freek Kapteijn,[a] Ferdinand Grozema,[b] Arjan Houtepen,[b] Jorge Gascon,[a] Johannes Hunger,[d] and Monique A. van der Veen*[a]

Recently, MIL-125(Ti) and NH_2-MIL-125(Ti), two titanium-based metal–organic frameworks, have attracted significant research attention in the field of photocatalysis for solar fuel generation. This work reveals that the differences between these structures are not only based on their light absorption range but also on the decay profile and topography of their excited states. In contrast to MIL-125(Ti), NH_2-MIL-125(Ti) shows markedly longer lifetimes of the charge-separated state, which improves photoconversion by the suppression of competing decay mechanisms. We used spectroelectrochemistry and ultrafast spectroscopy to demonstrate that upon photoexcitation in NH_2-MIL-125(Ti) the electron is located in the Ti-oxo clusters and the hole resides on the aminoterephthalate unit, specifically on the amino group. The results highlight the role of the amino group in NH_2-MIL-125(Ti), the electron donation of which extends the lifetime of the photoexcited state substantially.

Introduction

Our society is currently facing the challenge of fossil fuel depletion. Moreover, the utilization of such fuels also results in CO_2 emissions, which leads to climate change. In this context, solar-driven hydrogen production from water is very attractive to provide a long-term solution for sustainable solar energy conversion and storage,[1] yet efficiencies are still too low for practical application.[2]

Metal–organic frameworks (MOFs) are promising materials for gas separation and storage,[3] drug delivery,[4] chemical sensing,[5] and membrane technologies.[6] Recently, they have emerged as prospective alternative photocatalysts to more traditional materials such as TiO_2 or other semiconductors.[7] The unprecedented tunability of MOFs, typically characteristic of molecular (photo)catalysts, combined with the durability and recyclability of heterogeneous systems shows potential for a bright future in photocatalysis.

Notably, the number of reported MOFs based on earth-abundant elements that demonstrate photocatalytic activity is still increasing. To date, a variety of photocatalytic reactions, which include the most relevant for environmental concerns such as CO_2 reduction,[8] H_2 evolution,[9] and the oxidation of various pollutants,[10] have been catalyzed by frameworks based on metals such as Ti,[11] Zr,[12] Zn,[13] and Fe.[14] However, their performance is limited compared to that of state-of-the-art photocatalysts.[15] A fundamental understanding of photocatalysis by MOFs has the potential to advance this field significantly. If we consider that the oxygen half reaction is the kinetic bottleneck in the water splitting reaction,[16] it would be particularly interesting to unravel the pathway experienced by the photogenerated holes of MOFs such that more efficient oxidation catalysts for this reaction can be designed. This has remained elusive so far.

In this work, we focus on two MOFs based on titanium, MIL-125(Ti) and NH_2-MIL-125(Ti) (Figure 1). These two frameworks are isoreticular, which means that their structure and the crystallographic identity are not affected by the difference in the organic linkers that constitute the MOF. NH_2-MIL-125(Ti) is of great interest as it is one of the most reported MOFs in this field because of its successful application in visible-light photocatalysis.[8a, 9a, 17]

MIL-125(Ti) was reported for the first time by Férey and coworkers in 2009.[18] In the first publication, the authors assessed

[a] J. G. Santaclara,[+] M. A. Nasalevich,[+] Dr. S. Castellanos, Prof. F. Kapteijn, Prof. J. Gascon, Dr. M. A. van der Veen
Catalysis Engineering, Department of Chemical Engineering
Delft University of Technology
Julianalaan 136, 2628 BL Delft (The Netherlands)
E-mail: M.A.vanderVeen@tudelft.nl

[b] Dr. W. H. Evers, F. C. M. Spoor, Prof. L. D. A. Siebbeles, Dr. F. Grozema, Dr. A. Houtepen
Optoelectronic Materials, Department of Chemical Engineering
Delft University of Technology
Julianalaan 136, 2628 BL Delft (The Netherlands)

[c] Dr. W. H. Evers
Kavli Institute of Nanoscience
Delft University of Technology
Lorentzweg 1, 2628 CJ Delft (The Netherlands)

[d] Dr. K. Rock, Dr. J. Hunger
Max Planck Institute for Polymer Research
Ackermannweg 10, 55128 Mainz (Germany)

[+] These authors contributed equally to this work.

Supporting Information for this article is available on the WWW under http://dx.doi.org/10.1002/cssc.201501353.

This publication is part of a Special Issue on the "Chemistry for Energy Conversion and Storage" conference in Berlin, Germany. To view the complete issue visit: http://dx.doi.org/10.1002/cssc.v9.4.

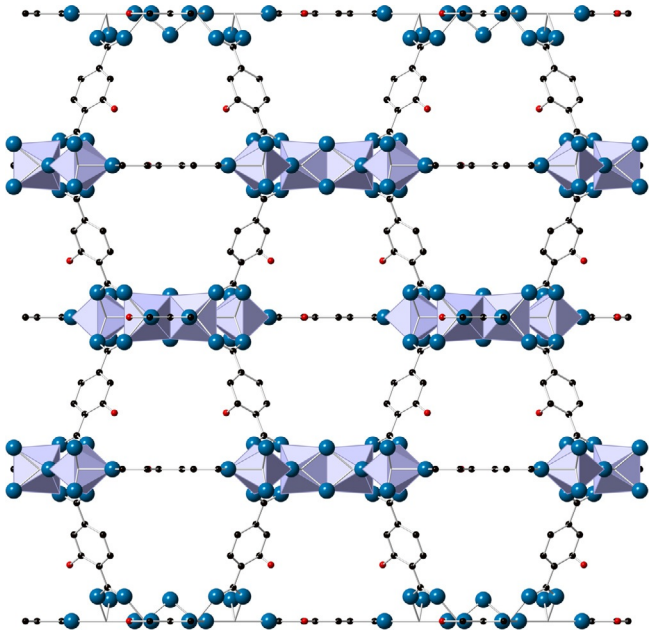

Figure 1. Crystal structure of X-MIL-125(Ti). View along (1 0 0). Red balls denote X, MIL-125(Ti) X = H; NH_2-MIL-125(Ti) X = NH_2. The orientation of the NH_2 groups with respect to each other cannot be determined by XRD.

the catalytic activity of MIL-125(Ti) in the oxidation of alcohols prompted by the analogy between the Ti-based MOF and the most studied photocatalyst TiO_2. However, the catalyst is only active under UV irradiation, which restricts its applicability in solar-driven photocatalysis. Later, the remarkable tunability of MOFs came into play: MIL-125(Ti) was synthesized using 2-aminoterephthalic acid (ATA) instead of terephthalic acid as the linker.[8a,19] The additional NH_2 group in the aromatic system of the linker yielded a framework sensitive to visible-light irradiation, named NH_2-MIL-125(Ti). Although the two MOFs are isoreticular, they possess some distinct properties, such as surface area and light absorption (Figures S1 and S2 a). It is often assumed that from a photocatalytic point of view the biggest difference between both systems is that the NH_2-functionalized version of the MOF is able to absorb lower-energy photons. However, in this work we demonstrate that the difference in photoexcitation is much more profound and is not limited to the light absorption profiles.

To exploit the rich potential of NH_2-MIL-125(Ti), in this study we address a set of fundamental questions related to how the presence of the amino group modifies the excited states promoted by light absorption compared to the nonaminated analog.

It is commonly accepted that photoexcitation in MIL-125(Ti) proceeds through ligand-to-metal charge transfer (LMCT).[9a,11,20] This implies that the highest occupied crystal orbital (HOCO) of MIL-125(Ti) resides on the organic linker, whereas the lowest unoccupied crystal orbital (LUCO) is localized largely on the titanium oxo cluster.[21] Such excitation promotes an electron from the linker to the metal to reduce it to Ti^{3+}. These species have been detected by EPR spectroscopy.[9a,11,18] However, although the localization of photogenerated holes is critical to design oxidation catalysts for reactions (i.e., water splitting) the pathway experienced by the photogenerated hole is less evident. Walsh and Catlow modeled photoexcitation in MIL-125(Ti) and found that the removal of an electron from the organic-defined HOCO is likely to result in the formation of hydroxyl radicals or an oxygen vacancy by O_2 release.[21] The oxygen atom involved in both processes is most probably the bridging oxydo ligand of the titanium oxo clusters.

A different process might occur in the case of NH_2-MIL-125(Ti). The NH_2 group of ATA carries a lone pair that can donate an electron relatively easily. Amines are well-known donors, and the formation of N-centered radical cations is not uncommon.[22]

In the present study, we resolve the localization of the photogenerated holes in NH_2-MIL-125(Ti) by a combination of spectroscopic techniques. The presence of the amino groups leads to a drastically slower decay of the photoexcited state with respect to that of MIL-125(Ti). The increase of the lifetime if electron-donating substituents are used on the organic linker is of great interest for the rational design of MOFs as photocatalysts. Moreover, the localization of the hole in the amine group provides knowledge upon which to base this rational design of MOF-based catalysts that fully exploit their oxidative power.

Results and Discussion

MIL-125(Ti) and NH_2-MIL-125(Ti) were synthesized according to protocols reported elsewhere.[19,20] We obtained MIL-125(Ti) and NH_2-MIL-125(Ti) that appear white and yellow, respectively, and possess large total pore volumes in line with previous reports (Figure S1).[19] Powder XRD showed that the MOFs have a high crystallinity, and no crystalline impurities were detected (Figure S2). The structures of MIL-125(Ti) and NH_2-MIL-125(Ti) are illustrated in Figure 1. These frameworks consist of octameric $Ti_8O_8(OH)_4$ clusters as nodes that are interconnected by the corresponding linkers to form a centered cubic structure.[18] Despite the identical crystal structure, some of the properties are remarkably different as a result of the additional substituent in the aromatic system of the terephthalate in the case of NH_2-MIL-125(Ti). The presence of the $-NH_2$ group, which holds a lone electron pair on the N atom, implies changes in the hydrophilicity and basicity compared to the bare aromatic linker. Importantly for photocatalysis, the lowest-energy optical absorption bands differ by circa 100 nm: MIL-125(Ti) has λ_{max} of 290 nm, whereas NH_2-MIL-125(Ti) absorbs visible light at λ_{max} = 380 nm (Figure 2 a).

Efforts have been made to push the absorption of photocatalytic systems into the visible region of the spectrum to utilize solar energy efficiently.[23] Clearly, an enhancement of the uptake of sunlight is only worthwhile if the redox potentials of the photogenerated charges are sufficient to drive the desired chemistry.

Apart from this requirement, the kinetics of the photoexcited states in MIL-125(Ti)-type MOFs have a profound effect on the efficiency of the photocatalysis. For an effective transfer of

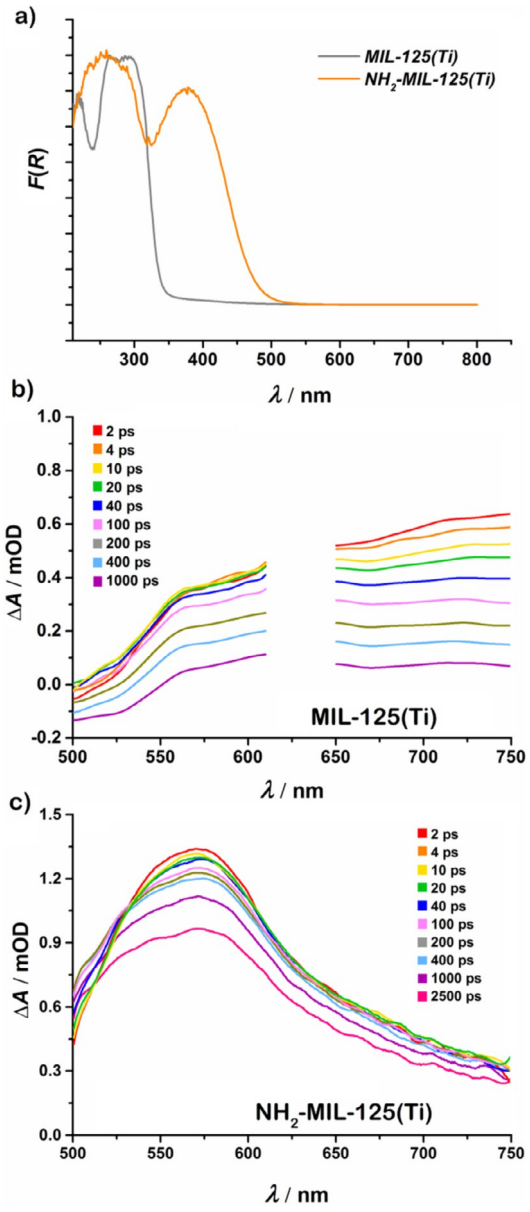

Figure 2. a) Diffuse reflectance UV/Vis spectra of the two catalysts: MIL-125(Ti) (grey), NH2-MIL-125(Ti) (orange). b) Transient spectra of MIL-125(Ti) in water upon excitation at 315 nm pump and c) NH_2-MIL-125(Ti) in water upon excitation at 400 nm pump. The remnant of the 630 nm light used to generate 315 nm light by second-harmonic generation in the pump beam overwhelms the transient spectra between $\lambda = 610$–650 nm, hence this part of the spectrum is omitted. A fast Fourier transform filter was applied to the experimental data and is shown as a trend for a more clear visualization.

the light-induced charges to a reactant, the lifetime of the charge-separated state needs to be sufficiently long to compete with other decay mechanisms of the photoexcited state. To assess the decay profiles of both MOFs, we performed ultrafast transient absorption (TA) spectroscopy.

In a typical TA experiment, an excitation laser pulse (pump) promotes a fraction of the chromophores to an electronically excited state. After a certain delay (τ), a weak probe pulse is sent through the excited sample, from which the transmission spectrum is detected. By subtracting the unpumped transmission spectrum of the probe, a difference absorption spectrum $\Delta A(\lambda,\tau)$ for the time delay τ is obtained. We used pulses of ~150 fs to obtain difference spectra $\Delta A(\lambda,\tau)$ with a sub-picosecond time resolution. This ultrafast time scale allows us to collect information on the dynamic processes that occur in the exposed system[24] and to probe the very first dynamics of the photoexcited state.

In general, the difference spectra contain contributions from the following processes: a) depletion of the ground state to lead to a negative ΔA called "ground state bleach"; b) redshifted from the ground state bleach, a negative ΔA may be caused by stimulated emission; c) a positive ΔA caused by excited state absorption; d) a positive ΔA caused by reactions of the excited state to result in charge-separated states, triplet states, among others.[24]

Two types of probe beams were employed in this study. The type 1 probe assesses visible-light absorption. The TA in this configuration is ideally suited to follow charge transfer to/from the metal center because it provides direct information on the excited redox-active states of the MOFs. The type 2 probe provides a mid-IR absorption spectrum. Transient IR absorption spectroscopy is able to trace the motion of photogenerated charge carriers through various functional organic groups of modular materials.[25]

The transient absorption spectra of MIL-125(Ti) and NH_2-MIL-125(Ti) are presented in Figure 2b and c, respectively. With the application of water splitting in mind, we selected water as the solvent. TA spectra of NH_2-MIL-125(Ti) were also measured in DMF to compare the obtained results in a solvent of different polarity (Figure S8). The MOFs were excited at wavelengths as close as possible to their respective absorption maxima ($\lambda =$ 315 and 400 nm).

In the case of MIL-125(Ti), the observed transient signal covers the whole $\lambda = 500$–750 nm range and decays rapidly to the ground state after the pump pulse excitation. We also detected stimulated emission that leads to negative absorption (below $\lambda = 525$ nm). In contrast, NH_2-MIL-125(Ti) shows a substantially different behavior. The excitation results in an intense transient signal with a maximum at $\lambda = 570$ nm, a shoulder at $\lambda = 530$ nm, and a somewhat broad additional band at $\lambda =$ 500–750 nm. It is clear that the excited state absorption of NH_2-MIL-125(Ti) exhibits much slower decay than that observed for MIL-125(Ti) (Figure 3). Indeed, more than 70% of the signal intensity for NH_2-MIL-125(Ti) remains after 3 ns, the time window of the measurement, versus 10% for MIL-125(Ti).

Notably, the information extracted from the TA analysis is of great relevance as the kinetics of the excited state decay can have a profound impact on the photocatalytic performance. More efficient photocatalysis is expected if photoexcited charges have a longer lifetime, whereas the lifetime of the excited state of MIL-125(Ti) may be too short to allow the efficient utilization of the generated charge carriers.

In addition to the charge recombination rates, the localization of the photogenerated charge carriers in MIL-125(Ti) and NH_2-MIL-125(Ti) is critical for the rational design of photocatalysts. It is accepted that in both MOFs the photogenerated electron is mainly centered on Ti.[9a] Moreover, LMCT in MIL-

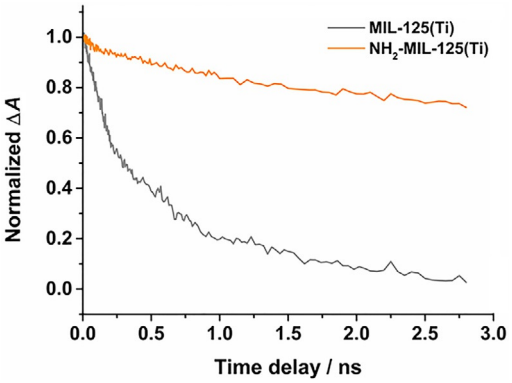

Figure 3. Comparison of the time traces of MIL-125(Ti) (grey) and NH_2-MIL-125(Ti) (orange) in water in the range $\lambda = 560–610$ nm.

125(Ti)-type materials has been demonstrated clearly by EPR spectroscopy,[9a,11] flash photolysis,[26] and theory.[21] The detection of Ti^{+3} is straightforward because of its paramagnetic nature and the clear signatures of these species in the visible-light region, regardless of the surrounding structure.[18,20,27] However, the localization of the hole remains rather unclear. As discussed above, with the help of DFT, Walsh and Catlow revealed the importance of the organic linker in the photogeneration of the hole for MIL-125(Ti).[21] To the best of our knowledge, no such information has been reported for NH_2-MIL-125(Ti). Indeed, inducing a LMCT implies that the positively charged hole is localized mainly on the organic linker, yet there is no clear evidence for this. Here this issue is addressed through the analysis of the different spectral features of the photoexcited states obtained from TA by spectroelectrochemistry.

Along with the slower decay kinetics, TA spectra of NH_2-MIL-125(Ti) differ from those of its nonaminated counterpart in the clear dominance of a peak centered at $\lambda = 570$ nm. If we assume that LMCT occurs in both MOFs, the differences in their respective TA spectra might arise from the distinct absorption features of the holes localized in the two different linkers. To detect the optical changes associated with the injection of a hole in the NH_2-MIL-125(Ti) amino linker, a model molecule was used in spectroelectrochemistry experiments. In situ absorption spectra of aminoterephthalate dimethyl ester were recorded upon its electrochemical oxidation (Figure 4a). Immediately after the anodic current starts, the bleaching of the bands at $\lambda = 250$ and 365 nm is recorded together with the growth of new bands at $\lambda = 300$ and 530 nm. We assign these initial changes, which exhibit clear isosbestic points at $\lambda = 402$, 334, and 267 nm, to the initial formation of the aminoterephthalatic radical cation.[26] Such radical species further react, most likely through dimerization,[28] to lead to irreversible oxidation and permanent alterations of the optical spectrum (Figure S17). Notably, if the linker is incorporated in the MOF lattice, such dimerization reactions between radical cations cannot occur and allow a reversible cycle of the charge separation/recombination to lead to photocatalytic activity.

The spectral features of the aminoterephthalate radical cation can be recognized clearly in the TA spectrum of NH_2-

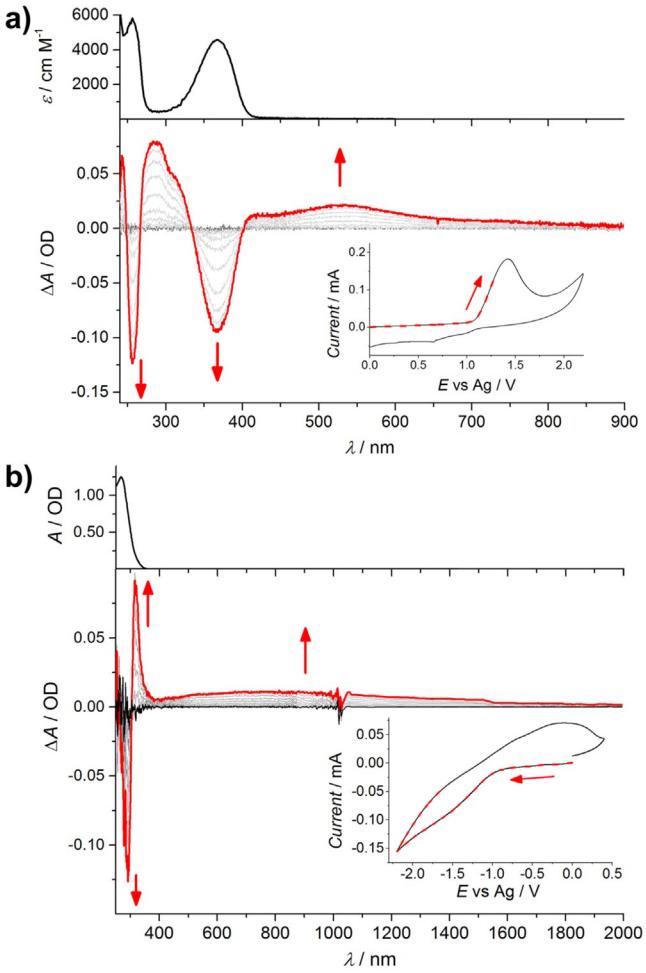

Figure 4. Absorption spectral changes of a) aminoterephthalate dimethyl ester in acetonitrile and b) $Ti_8O_8[OOCC(CH_3)_3]_{16}$ soluble oxo clusters in dichloromethane upon oxidation and reduction, respectively. Ground-state absorption spectra are shown on top of each spectroelectrochemical measurement. Insets display the registered cyclic voltammogram and the voltage range that corresponds to the shown spectra is highlighted by red dashes.

MIL-125(Ti) (Figure 2c and Figure S27). The redshift of the maximum (from $\lambda = 530$ nm in the linker to $\lambda = 570$ nm in the MOF) is in line with that observed in the ground-state spectra of the MOF (Figure 2a) and the linker (Figure 4a top). Thus, we conclude that a hole is located on the linker in the excited state.

To unequivocally find the optical fingerprint of the Ti^{3+} species in these MOFs, we performed the same experiment with inverted bias and with soluble titanium oxo clusters. Such oxo clusters, with the molecular formula $Ti_8O_8[OOCC(CH_3)_3]_{16}$, consist of well-defined ring-shaped Ti octamers linked by the carboxylic groups of pivalic acid ligands and are used as precursors in the synthesis of MIL-125(Ti).[20]

Upon the application of negative potentials, the generation of cathodic current was accompanied by the appearance of a broad band with a smooth maximum around $\lambda = 750$ nm and a tail that covers the near-IR region together with the bleaching of the band at $\lambda = 268$ nm (Figure 4b). Such changes were fully reversible upon reversing the applied potential (Fig-

ure S26). Thus, in line with previous studies in which $Ti^{3+/4+}$ mixed valence states are identified by the detection of broad bands that cover range of $\lambda = 400$ nm to near-IR,[18,27c,d] we assign the $\lambda = 400$–2000 nm positive ΔA shown in Figure 4b to the reduced species of the titanium oxo clusters. Such a different absorption profile is also present in the TA spectra of MIL-125(Ti) (Figure 2b) and overlaps with the radical cation absorption band in NH_2-MIL-125(Ti) (Figure 2c). This indicates that electrons are indeed injected into the inorganic scaffolds in the nonaminated and aminated MIL-125(Ti), although they exhibit different decays. Thus spectroelectrochemical analysis gives strong evidence for the LMCT character of the NH_2-MIL-125(Ti) photoexcited state through the detection of the linker radical cation ($\lambda = 570$ nm) and the reduced Ti-oxo cluster ($\lambda =$ 500–750 nm broad band) absorption fingerprints. This demonstrates that the behavior observed in the MOF is a clear combination of the behavior shown by its main components, which again suggests that MOFs should be considered as an array of self-assembled molecular catalysts rather than as classical semiconductors.

To understand how the photogenerated oxidative power of the NH_2-MIL-125(Ti) framework may be harnessed and more precisely localize the photoexcited hole on the organic linker, a mid-IR probe was used. Indeed, the region of the mid-IR that we examined ($\tilde{\nu} = 1250$–3620 cm^{-1}; Figure 5) solely probes the

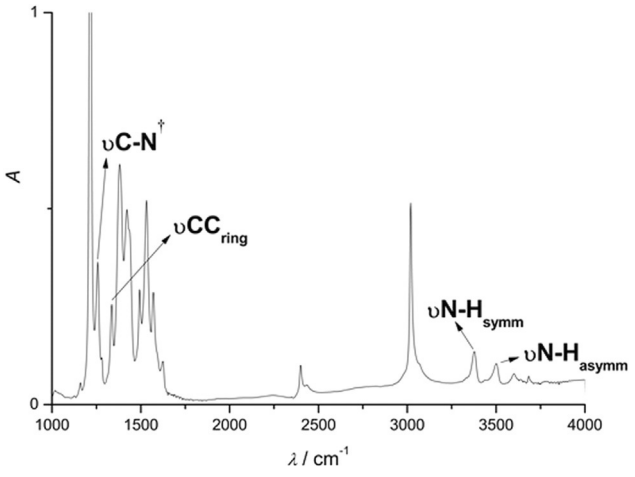

Figure 5. FTIR spectrum of NH_2-MIL-125(Ti) in $CHCl_3$. Vibrations discussed in the main text are shown. This is most likely a combination band of vibrations but, for better visualization, only the contribution of the νC–N is shown. All the assignments can be found in Table S1.

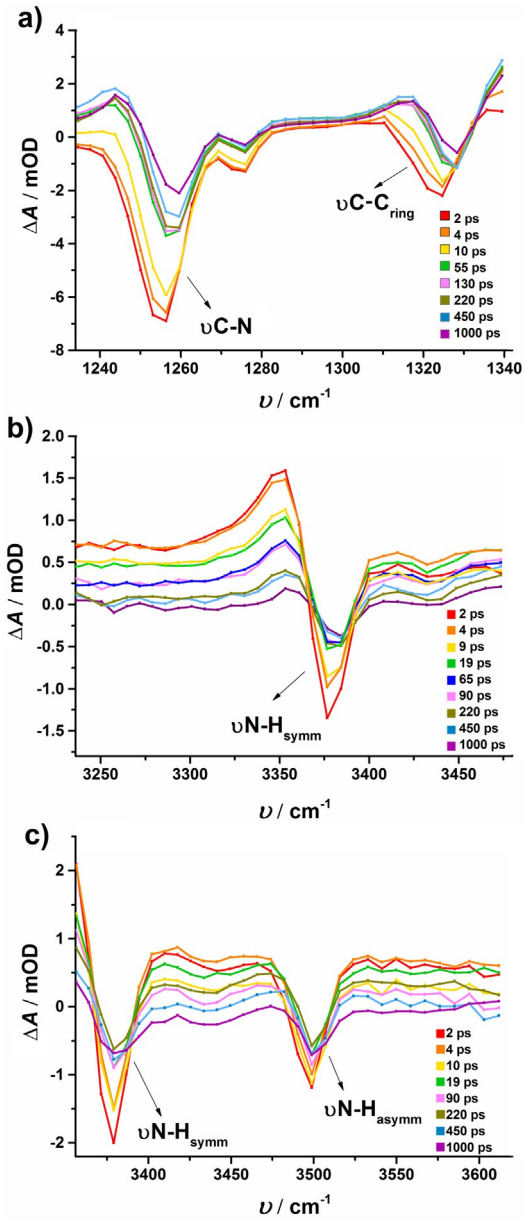

Figure 6. Differential transient absorption spectra for NH_2-MIL-125(Ti) in $C_2H_2Cl_4$ as solvent upon excitation at 400 nm: a) C–N stretching vibration region, b) N–H and c) N–H symmetric stretching vibration region. Lines are depicted for a better visualization of the data. Although ΔA is different for b) and c), the N–H symmetric vibration is depicted in both plots. This is most likely a combination band of vibrations but, for better visualization, only the contribution of the νC–N is shown. The complete assignment can be found in Table S1.

organic vibrations of the structure. For this purpose, the MOF was immersed in an IR-transparent solvent and assessed by a mid-IR probe after an excitation pulse at $\lambda = 400$ nm, again with a sub-picosecond time resolution. Polar (D_2O, $\tilde{\nu} = 1350$–1610 cm^{-1}) and apolar ($C_2H_2Cl_4$, $\tilde{\nu} = 1250$–3620 cm^{-1}) solvents were used. Except for solvochromatic shifts, similar transient spectra and time dynamics are observed in both media (Figure 6, Figures S10–S24). Hence, it is likely that the spectra of NH_2-MIL-125(Ti) are representative of the situation in water, also for the ranges for which $C_2H_2Cl_4$ was the sole transparent solvent for the IR probe. Although we expected to obtain different spectra and kinetics if we used solvents with different polarities (generally, more polar media facilitate charge-transfer processes)[29] our results may be associated with the less efficient solvation of the porous material compared to that of discrete molecules.

The transient mid-IR probe spectra specifically for the regions that correspond to the amino group are shown in Figure 6 [see Figure 5 for the ground-state mid-IR absorbance

spectrum of NH_2-MIL-125(Ti)]. The N–H and C–N bond stretching vibrations show pronounced bleaching in the TA spectra. The transient spectra at $\tilde{\nu}=3000$–$3610\ cm^{-1}$ (Figure 6b and c, Figures S21 and S23) show a flat featureless induced absorption, which likely originates from the broad visible-light absorbance that extends far into the near-IR with the presence of Ti^{3+} in the Ti-oxo clusters (Figure 4b).

Along the different spectral regions, we find strong coupling of the excited state to molecular vibrations associated with the amine group of the MOF structure. At $\tilde{\nu}=3485\ cm^{-1}$, which corresponds to the characteristic frequency of the N–H asymmetric stretching vibration (Figure 6c), a long-lived bleaching signal is observed, which can be explained by a reduction of the transition dipole moment of the vibration upon photoexcitation. In contrast, at the N–H symmetric frequency ($\tilde{\nu}=3380\ cm^{-1}$; Figure 6b) a redshifted induced absorption is observed adjacent to the bleaching signal at the fundamental frequency indicative of a redshift of the N–H stretching band.

Notably, for the oxidized aniline radical with respect to neutral aniline, a more pronounced redshift of the symmetrical N–H stretch is reported than for the asymmetrical N–H stretch ($\tilde{\nu}=40$ vs. $20\ cm^{-1}$), in addition to a higher IR intensity of the symmetrical N–H stretch than the asymmetrical N–H stretch of the radical. In the positive radical of aniline, the reduced electron density is most pronounced on the N atom.[30] This is in line with the transient mid-IR spectra obtained and a first indication of reduced electron density on the N atom of NH_2-MIL-125(Ti). A significant bleach can be seen in the spectra shown in Figure 6a that corresponds to the bleach of the ground-state vibration of the combination band dominated by the C–N stretching vibration at $\tilde{\nu}=1257\ cm^{-1}$ (Figure 5) and a bleach that corresponds to the ground-state C–C_{ring} vibration at $\tilde{\nu}=1334\ cm^{-1}$, which indicates the ground-state depletion of these vibrations.

Notably, at most resonances in the IR spectra the associated dynamics equilibrated on a timescale of ~20 ps and the associated transient spectra remain constant within the time frame of the experiment (e.g., the band at $\tilde{\nu}=1325\ cm^{-1}$ in Figure 7 and Figures S10–S12). This indicates that the MOF structure is relaxing on rather fast timescales because of vibrational cooling. Remarkably, only the vibrations that are related to the C–N–H_2 group show adjacent slower dynamics: the bands in the transient spectra at $\tilde{\nu}=3485$, 3380, and $1256\ cm^{-1}$ (N–H asymmetric stretch, N–H symmetric stretch, and C–N stretch) do not plateau within 1 ns, the experimentally accessible delay time range (e.g., the band at $\tilde{\nu}=1256\ cm^{-1}$ in Figure 7 and Figure S10). If we compare this with the time dependence of the transient visible spectra (Figure 7), we see similar slower time dynamics. As we were able to assign the band around $\lambda=570$ nm to the hole previously, this is a clear indication that the C–N–H_2-related vibrations are associated with the hole. After 5 ns, the resonances associated with C–N–H_2 are also equilibrated (Figure S11). This longer-lived state is potentially caused by intersystem crossing to a triplet state, which is common for aniline derivates.[31]

The resemblance of the time dynamics between the resonances of the C–N–H_2 vibrations and the visible transient spectrum associated with the hole and the resemblance of the transient mid-IR spectra with that of the aniline radical reveal a positively charged vacancy most likely localized on the NH_2 group of the aminoterephthalate. Therefore, the electron-donating character of the amino group contributes to the stabilization of the photoexcited state with respect to MIL-125(Ti).

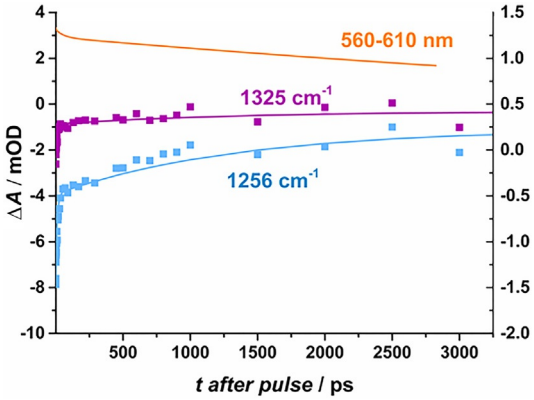

Figure 7. Representative time traces of NH_2-MIL-125(Ti) upon excitation at 400 nm in $C_2H_2Cl_4$ recorded at $\tilde{\nu}=1256$ (blue) and $1325\ cm^{-1}$ (purple): experimental data (squares) and model fit (line). The orange line (which corresponds to the right *y* axis) represents the time traces in the $\lambda=560$–610 nm range in water (Figure 3 orange, experimental data). The plot starts at 1 ps to remove the points related to the coherent artifact.

Conclusions

The kinetics of the photoexcitation process of two titanium metal–organic frameworks [MOFs; MIL-125(Ti) and NH2-MIL-125(Ti)] were elucidated. These MOFs show, apart from their thermodynamic differences that lead to dissimilar light absorption profiles, a vast contrast in their photoexcited kinetic behavior. The excited state, which results from a LMCT transition, has a remarkably longer lifetime in NH_2-MIL-125(Ti).

Our results clarify the contributions of the organic and inorganic subunits to the formation of the charge-separated state. Spectroelectrochemistry performed on the soluble models of the organic and inorganic NH_2-MIL-125(Ti) constituents gave further insights into the transient absorption experiments. The results point to the localization of the hole on the aminoterephthalate unit and of the electron on the Ti-oxo clusters. Furthermore, ultrafast mid-IR spectra evidenced that the photogenerated hole resides on the amino group.

Thus, the amino group, which acts as a hole stabilizer in NH_2-MIL-125(Ti), prolongs the lifetime of the photoexcited state considerably compared to that of MIL-125(Ti). The NH_2 group sensitizes MIL-125(Ti) to visible light and enables the capture of a larger fraction of solar light without the use of expensive noble metals while also improving the kinetics of the photoexcitation. To allow photogenerated charges to be used effectively in photocatalytic reactions, such as solar fuel generation, their lifetime needs to be sufficient. These results provide us with important insight into how to improve photocatalytic metal–organic frameworks. In particular, our findings encourage the design of MIL-125(Ti)-type structures with one or

multiple strong electron donor groups to improve their photocatalytic performance. Moreover, the knowledge that the hole resides on the amino group allows us to create a rational design scheme to harness these holes for the oxygen evolution half reaction.

Experimental Section

Materials and reagents

All chemicals were purchased from Sigma Aldrich and used without further purification.

Synthesis

MIL-125(Ti) was synthesized according to a method reported previously.[19] Typically, terephthalic acid (3.53 g) and anhydrous DMF (56 mL) were mixed and placed in a round-bottomed flask. The mixture was heated at 105 °C for 1 h to dissolve the acid and remove the residual water. With the temperature of the solution kept at 105 °C, anhydrous methanol (14 mL) was added, and a reflux condenser was fitted. The solution was heated under stirring for 1 h, after which titanium isopropoxide (4.2 mL) was added. The resulting mixture was heated to reflux with stirring for 72 h at 100 °C. After cooling to RT and filtration of the mixture, a white solid was isolated, which was washed with DMF for 24 h at 155 °C and then methanol at 100 °C. The white product was dried in air at 100 °C to remove methanol from the pores.

NH_2-MIL-125(Ti) was synthesized using a protocol reported by Walsh and co-workers.[20] Typically, 2-aminoterephthalic acid (0.5 g, 2.76 mmol) was dissolved in a mixture of anhydrous DMF (16 mL) and anhydrous methanol (4 mL) at RT in a glovebox. Titanium isopropoxide (0.55 mL, 1.93 mmol) was added, and the mixture was placed in an autoclave. The autoclave was sealed and heated for 72 h at 110 °C. The obtained yellow solid was collected by filtration, dispersed in fresh DMF, and heated at 110 °C overnight to remove residual linker. Then, the same procedure was repeated using methanol for 6 h at 80 °C. Finally, the solid was dried in air at 80 °C.

Characterization

Powder XRD patterns were recorded by using a Bruker-AXS D5005 with CoK_α radiation.

Nitrogen physisorption measurements were performed by using a Tristar II 3020 Micromeritics unit at 77 K. Before the experiment, the samples were degassed for 16 h at 423 K under vacuum. The BET areas were calculated using intervals to allow positive BET constants.[32] The total pore volumes were calculated at a relative pressure of 0.9.

Thermogravimetric analysis (TGA) was performed by using a Mettler Toledo TGA/SDTA851 system under air flow (60 mL min^{-1}) at a heating rate of 10 K min^{-1} to 1073 K.

Diffuse reflectance UV/Vis spectra were collected by using a PerkinElmer Lambda 900 spectrophotometer equipped with an integrating sphere ("Lambsphere") in the $\lambda = 200$–800 nm range. $BaSO_4$ was used as a white standard.

The optical setup for spectroelectrochemistry comprised a Deuterium-Halogen lamp DH-2000 as light source, a USB2000 UV/Vis spectrometer, and a NIRQUEST near-IR spectrometer, all from Ocean Optics Inc. The potential was applied by using a CH Instruments Analyser CHI832B as the potentiostat. An optically transparent thin-layer electrochemical (OTTLE) cell fabricated by Spectroelectrochmistry Reading (University of Reading)[33] provided with a three-electrode set that consisted of a Pt minigrid working electrode (32 wires cm^{-1}), Pt minigrid auxiliary electrode, and Ag wire pseudo-reference electrode melt-sealed in a modified polyethylene spacer (≈0.2 mm thickness) was used as the measuring cell. $LiClO_4$ in acetonitrile (0.1 M) and $(NtBu_4)BF_4$ in dichloromethane (0.1 M) were used as electrolytes for aminoterephthalate dimethyl ester and $Ti_8O_8[OOCC(CH_3)_3]$, respectively. All solutions were prepared under glovebox conditions to avoid the presence of oxygen.

Femtosecond transient absorption spectroscopy was performed. Samples for visible (Vis)-pump visible-probe measurements were excited by 180 fs pulses at $\lambda = 400$ nm generated by using a YKGBW oscillator (Light Conversion, Pharos SP) at $\lambda = 1028$ nm through nonlinear frequency mixing in an optical parametric amplifier (OPA) and second harmonics module (Light Conversion, Orpheus). A small fraction of the $\lambda = 1028$ nm fundamental beam was split off to generate the broadband probe spectrum in a sapphire (500–1600 nm) crystal. The probe pulse was delayed relative to the pump using a delay stage with maximum delay of 3 ns. The pump and probe pulses overlap on the sample position at an angle of ~8°, after which the probe light is led to a detector suitable for the probe spectrum selected (Ultrafast Systems, Helios). To prevent multiple photon absorption processes, the pump fluence was set sufficiently low to allow us to study single exciton dynamics. Typically, MOF (50 mg) was dispersed in the solvent (14 mL) and sonicated for 30 min. To separate large particles (>100 nm), the suspension was then centrifuged for 30 min at 6000 rpm. The supernatant was placed in a 2 mm stirred quartz cuvette for the measurements.

Vis-pump IR probe experiments were performed by using a regenerative Ti:Sapphire amplified laser system (Spitfire Ace, Spectra Physics) to provide pulses at $\lambda = 800$ nm with a duration of 35 fs and a pulse energy of 5 mJ at a repetition rate of 1 kHz. Commercial optical parametric amplifiers (TOPAS-C, Spectra-Physics) were pumped with 1.5 mJ of the $\lambda = 800$ nm pulses. The signal and idler pulses from one TOPAS-C were used in a difference frequency mixing process in a silver gallium disulfide ($AgGaS_2$) crystal, resulting in ~8 μJ tunable IR pulses with a full width at half maximum (FWHM) of 300 cm^{-1}. A wedged CaF_2 window was used to generate a probe and a reference pulse from the output of the OPA, and the reflection of the front side was used as the probe pulse and the back-reflection was used as a reference pulse. A second portion of the $\lambda = 800$ nm pulses was frequency-doubled in a β-barium borate crystal to yield visible pump pulses with a central wavelength of 400 nm. A translational stage was used to control the timing of the Vis-pump pulses relative to the IR probe pulses. A mechanical chopper was used to block every second pump pulse, which allows active background subtraction. The pump, probe, and reference pulses were focused into the sample, and the pump and the probe pulses were spatially overlapped. The probe and the reference pulses were recollimated and spectrally dispersed by using an imaging spectrograph (Horiba Triax 180). The intensities I were detected on two separate lines of a 3×32 mercury-cadmium-telluride (MCT, Infrared Associates) detector array. The pump-induced absorption changes were thus given as $\Delta A = -\ln[I_{probe} \cdot I_{reference,0} / (I_{probe,0} \cdot I_{reference})]$, in which the subscript 0 refers to the IR intensities recorded without pump excitation. For all the measurements, NH_2-MIL-125(Ti) (40 mg) was dried overnight at 423 K then dispersed in solvent (800 μL) and sonicated for 15 min.

Acknowledgements

M.N. acknowledges NRSCC for financial support. This work is part of the research program of the Foundation for Fundamental Research on Matter (FOM), which is part of the Netherlands Organization for Scientific Research (NWO). M.A.v.d.V. acknowledges FWO (Flanders) for financial support.

Keywords: amines · metal–organic frameworks · photochemistry · titanium · water splitting

[1] C. Acar, I. Dincer, *Int. J. Energy Res.* **2015**, *39*, 1757 – 1768.
[2] a) W. J. Youngblood, S.-H. A. Lee, K. Maeda, T. E. Mallouk, *Acc. Chem. Res.* **2009**, *42*, 1966 – 1972; b) G. F. Moore, G. W. Brudvig, *Annu. Rev. Condens. Matter Phys.* **2011**, *2*, 303 – 327.
[3] S. Ma, H.-C. Zhou, *Chem. Commun.* **2010**, *46*, 44 – 53.
[4] a) K. M. L. Taylor-Pashow, J. Della Rocca, Z. Xie, S. Tran, W. Lin, *J. Am. Chem. Soc.* **2009**, *131*, 14261 – 14263; b) R. C. Huxford, J. Della Rocca, W. Lin, *Curr. Opin. Chem. Biol.* **2010**, *14*, 262 – 268.
[5] C. Wang, D. Liu, W. Lin, *J. Am. Chem. Soc.* **2013**, *135*, 13222 – 13234.
[6] a) T. Rodenas, I. Luz, G. Prieto, B. Seoane, H. Miro, A. Corma, F. Kapteijn, F. X. Llabrés i Xamena, J. Gascon, *Nat. Mater.* **2015**, *14*, 48 – 55; b) B. Seoane, J. Coronas, I. Gascon, M. E. Benavides, O. Karvan, J. Caro, F. Kapteijn, J. Gascon, *Chem. Soc. Rev.* **2015**, *44*, 2421 – 2454.
[7] a) T. Zhang, W. Lin, *Chem. Soc. Rev.* **2014**, *43*, 5982 – 5993; b) M. Nasalevich, M. A. van der Veen, F. Kapteijn, J. Gascon, *CrystEngComm* **2014**, *16*, 4919 – 4926.
[8] a) Y. Fu, D. Sun, Y. Chen, R. Huang, Z. Ding, X. Fu, Z. Li, *Angew. Chem. Int. Ed.* **2012**, *51*, 3364 – 3367; *Angew. Chem.* **2012**, *124*, 3420 – 3423; b) D. Sun, Y. Fu, W. Liu, L. Ye, D. Wang, L. Yang, X. Fu, Z. Li, *Chem. Eur. J.* **2013**, *19*, 14279 – 14285.
[9] a) M. A. Nasalevich, R. Becker, E. V. Ramos-Fernandez, S. Castellanos, S. L. Veber, M. V. Fedin, F. Kapteijn, J. N. H. Reek, J. I. van der Vlugt, J. Gascon, *Energy Environ. Sci.* **2015**, *8*, 364 – 375; b) D. Sun, W. Liu, Y. Fu, Z. Fang, F. Sun, X. Fu, Y. Zhang, Z. Li, *Chem. Eur. J.* **2014**, *20*, 4780 – 4788.
[10] C.-C. Wang, J.-R. Li, X.-L. Lv, Y.-Q. Zhang, G. Guo, *Energy Environ. Sci.* **2014**, *7*, 2831 – 2867.
[11] Y. Horiuchi, T. Toyao, M. Saito, K. Mochizuki, M. Iwata, H. Higashimura, M. Anpo, M. Matsuoka, *J. Phys. Chem. C* **2012**, *116*, 20848 – 20853.
[12] a) J. Long, S. Wang, Z. Ding, S. Wang, Y. Zhou, L. Huang, X. Wang, *Chem. Commun.* **2012**, *48*, 11656 – 11658; b) C. Wang, Z. Xie, K. E. deKrafft, W. Lin, *J. Am. Chem. Soc.* **2011**, *133*, 13445 – 13454.
[13] a) J. Gascon, M. D. Hernandez-Alonso, A. R. Almeida, G. P. M. van Klink, F. Kapteijn, G. Mul, *ChemSusChem* **2008**, *1*, 981 – 983; b) M. Alvaro, E. Carbonell, B. Ferrer, F. Xamena, H. Garcia, *Chem. Eur. J.* **2007**, *13*, 5106 – 5112.
[14] K. G. M. Laurier, F. Vermoortele, R. Ameloot, D. E. De Vos, J. Hofkens, M. B. J. Roeffaers, *J. Am. Chem. Soc.* **2013**, *135*, 14488 – 14491.
[15] S. Wang, X. Wang, *Small* **2015**, *11*, 3097 – 3112.
[16] a) D. Gust, T. A. Moore, A. L. Moore, *Acc. Chem. Res.* **2009**, *42*, 1890 – 1898; b) M. H. V. Huynh, T. J. Meyer, *Chem. Rev.* **2007**, *107*, 5004 – 5064; c) J. P. McEvoy, G. W. Brudvig, *Chem. Rev.* **2006**, *106*, 4455 – 4483.
[17] M. A. Nasalevich, M. G. Goesten, T. J. Savenije, F. Kapteijn, J. Gascon, *Chem. Commun.* **2013**, *49*, 10575 – 10577.
[18] M. Dan-Hardi, C. Serre, T. Frot, L. Rozes, G. Maurin, C. Sanchez, G. Férey, *J. Am. Chem. Soc.* **2009**, *131*, 10857 – 10859.
[19] M. A. Moreira, J. C. Santos, A. F. P. Ferreira, J. M. Loureiro, F. Ragon, P. Horcajada, P. G. Yot, C. Serre, A. E. Rodrigues, *Microporous Mesoporous Mater.* **2012**, *158*, 229 – 234.
[20] C. H. Hendon, D. Tiana, M. Fontecave, C. Sanchez, L. D'arras, C. Sassoye, L. Rozes, C. Mellot-Draznieks, A. Walsh, *J. Am. Chem. Soc.* **2013**, *135*, 10942 – 10945.
[21] A. Walsh, C. R. A. Catlow, *ChemPhysChem* **2010**, *11*, 2341 – 2344.
[22] a) J. Hu, J. Wang, T. H. Nguyen, N. Zheng, *Beilstein J. Org. Chem.* **2013**, *9*, 1977 – 2001; b) M. Jonsson, J. Lind, T. E. Eriksen, G. Merenyi, *J. Am. Chem. Soc.* **1994**, *116*, 1423 – 1427.
[23] a) X. Chen, S. Shen, L. Guo, S. S. Mao, *Chem. Rev.* **2010**, *110*, 6503 – 6570; b) A. Kudo, Y. Miseki, *Chem. Soc. Rev.* **2009**, *38*, 253 – 278.
[24] R. Berera, R. Grondelle, J. T. M. Kennis, *Photosynth. Res.* **2009**, *101*, 105 – 118.
[25] J. B. Asbury, E. Hao, Y. Wang, H. N. Ghosh, T. Lian, *J. Phys. Chem. B* **2001**, *105*, 4545 – 4557.
[26] M. De Miguel, F. Ragon, T. Devic, C. Serre, P. Horcajada, H. García, *ChemPhysChem* **2012**, *13*, 3651 – 3654.
[27] a) C. Creutz, M. H. Chou, *Inorg. Chem.* **2008**, *47*, 3509 – 3514; b) P. Jeske, G. Haselhorst, T. Weyhermueller, K. Wieghardt, B. Nuber, *Inorg. Chem.* **1994**, *33*, 2462 – 2471; c) A. I. Kuznetsov, O. Kameneva, N. Bityurin, L. Rozes, C. Sanchez, A. Kanaev, *Phys. Chem. Chem. Phys.* **2009**, *11*, 1248 – 1257; d) G. K. Ramesha, J. F. Brennecke, P. V. Kamat, *ACS Catal.* **2014**, *4*, 3249 – 3254; e) J. Tory, B. Setterfield-Price, R. A. W. Dryfe, F. Hartl, *ChemElectroChem* **2015**, *2*, 213 – 217; f) S. Varaganti, G. Ramakrishna, *J. Phys. Chem. C* **2010**, *114*, 13917 – 13925.
[28] a) M. Kirchgessner, K. Sreenath, K. R. Gopidas, *J. Org. Chem.* **2006**, *71*, 9849 – 9852; b) E. T. Seo, R. F. Nelson, J. M. Fritsch, L. S. Marcoux, D. W. Leedy, R. N. Adams, *J. Am. Chem. Soc.* **1966**, *88*, 3498 – 3503; c) S. Sumalekshmy, K. R. Gopidas, *Chem. Phys. Lett.* **2005**, *413*, 294 – 299; d) M. Jin, Z. Yu, Y. Xia, *Russ. J. Electrochem.* **2006**, *42*, 964 – 968.
[29] J. D. Megiatto Jr., A. Antoniuk-Pablant, B. D. Sherman, G. Kodis, M. Gervaldo, T. A. Moore, A. L. Moore, D. Gust, *Proc. Natl. Acad. Sci. USA* **2012**, *109*, 15578 – 15583.
[30] P. M. Wojciechowski, W. Zierkiewicz, D. Michalska, *J. Chem. Phys.* **2003**, *118*, 10900 – 10911.
[31] a) H. Shimamori, A. Sato, *J. Phys. Chem.* **1994**, *98*, 13481 – 13485; b) X. Hou, P. Quan, T. Höltzl, T. Veszprémi, M. T. Nguyen, *J. Phys. Chem. A* **2005**, *109*, 10396 – 10402.
[32] M. F. De Lange, T. J. H. Vlugt, J. Gascon, F. Kapteijn, *Microporous Mesoporous Mater.* **2014**, *200*, 199 – 215.
[33] a) E. Hashem, J. A. Platts, F. Hartl, G. Lorusso, M. Evangelisti, C. Schulzke, R. J. Baker, *Inorg. Chem.* **2014**, *53*, 8624 – 8637; b) J. Tory, B. Setterfield-Price, R. A. W. Dryfe, F. Hartl, *ChemElectroChem* **2015**, *2*, 213 – 217; c) E. Hashem, J. A. Platts, F. Hartl, G. Lorusso, M. Evangelisti, C. Schulzke, R. J. Baker, *Inorg. Chem.* **2014**, *53*, 8624 – 8637; d) C. C. Ferrón, M. Capdevila-Cortada, R. Balster, F. Hartl, W. Niu, M. He, J. J. Novoa, J. T. López Navarrete, V. Hernández, M. C. Ruiz Delgado, *Chem. Eur. J.* **2014**, *20*, 10351 – 10359.

Received: October 7, 2015
Revised: November 27, 2015
Published online on February 12, 2016